High power and good beam quality of two-dimensional VCSEL array with integrated GaAs microlens array

Zhenfu Wang,[1,2] Yongqiang Ning,[1,*] Yan Zhang,[1,2] Jingjing Shi,[1,2] Xing Zhang,[1,2] Lisen Zhang,[1,2] Wei Wang,[1,2] Di Liu,[1,2] Yongsheng Hu,[1,2] Haibing Cong,[1,2] Li Qin,[1] Yun Liu,[1] and Lijun Wang[1]

[1]*Key Laboratory of Excited State Processes, Changchun Institute of Optics, Fine Mechanics and Physics, Jilin, Changchun 130033, China*

[2]*Graduate University of Chinese Academy of Sciences, Beijing 100039, China*

**ningyq@ciomp.ac.cn*

Abstract: High power and good beam quality of two-dimensional bottom-emitting vertical-cavity surface-emitting laser array with GaAs microlens on the substrate is achieved. Uniform and matched convex microlens is directly fabricated by one-step diffusion-limited wet-etching techniques on the emitting windows. The maximum output power is above 1W at continuous-wave operation at room temperature, and the far-field beam divergence is below 6.6°at a current of 4A. These properties between microlens-integrated and conventional device at different operating current are demonstrated.

OCIS codes: (140.3290) Laser arrays; (140.7260) Vertical cavity surface emitting lasers.

References and links

1. K. Iga, F. Koyama, and S. Kinoshita, "Surface emitting semiconductor lasers," IEEE J. Quantum Electron. **24**(9), 1845–1855 (1988).
2. M. Grabherr, M. Miller, R. Jager, R. Michalzik, U. Martin, H. J. Unold, and K. J. Ebeling, "High-Power VCSEL's: Single Devices and Densely Packed 2-D-Arrays," IEEE J. Sel. Top. Quantum Electron. **5**(3), 495–502 (1999).
3. J. Cui, Y. Ning, Y. Zhang, P. Kong, G. Liu, X. Zhang, Z. Wang, T. Li, Y. Sun, and L. Wang, "Design and characterization of a nonuniform linear vertical-cavity surface-emitting laser array with a Gaussian far-field distribution," Appl. Opt. **48**(18), 3317–3321 (2009).
4. J.-F. Seurin, C. L. Ghosh, V. Khalfin, A. Miglo, G. Xu, J. D. Wynn, P. Pradhan, and L. A. D'Asaro, "High-power high-efficiency 2D VCSEL arrays," Proc. SPIE **6908**, 690808 (2008).
5. J.-F. Seurin, G. Xu, V. Khalfin, A. Miglo, J. D. Wynn, P. Pradhan, C. L. Ghosh, and L. A. D'Asaro, "Progress in high-power high-efficiency VCSEL arrays," Proc. SPIE **7229**, 722903 (2009).
6. E. M. Strzelecka, G. D. Robinson, L. A. Coldren, and E. L. Hu, "Fabrication of refractive microlenses in semiconductors by mask shape transfer in reactive ion etching," Microelectron. Eng. **35**(1–4), 385–388 (1997).
7. F. Qi, and N. K. A. Bryan, "Investigation of hybrid microlens integration with vertical-cavity surface-emitting lasers for free-space optical links," Opt. Express **10**(9), 413–418 (2002).
8. Z. L. Liau, D. E. Mull, C. L. Dennis, R. C. Williamson, and R. G. Waarts, "Large-numerical-aperture microlens fabrication by one-step etching and mass-transport smoothing," Appl. Phys. Lett. **64**(12), 1484–1486 (1994).
9. G. M. Peake, S. Z. Sun, and S. D. Hersee, "GaAs microlens arrays grown by shadow masked MOVPE," J. Electron. Mater. **26**(10), 1134–1138 (1997).
10. Y.-S. Kim, J. Kim, J.-S. Choe, Y.-G. Roh, H. Jeon, and J. C. Woo, "Semiconductor microlenses fabricated by one-step wet etching," IEEE Photon. Technol. Lett. **12**(5), 507–509 (2000).
11. S.-H. Park, S. Lee, and H. Jeon, "Mode-Stabilized Operation in a Microlens-Integrated 980 nm Vertical-Cavity Surface-Emitting Laser," Opt. Rev. **13**(3), 146–148 (2006).

1. Introduction

Vertical-cavity surface-emitting lasers (VCSELs) have been proved as strong competitors to conventional edge-emitting semiconductor lasers as compact light sources in optical communication and interconnect with attractive properties such as low threshold current, wafer-level testing, compatibility with flip-chip bonding, and easy fabrication of two-dimensional arrays [1–3]. These features, together with its high-speed modulation, have made it widespread application in, for example, short-distance parallel fiber-optic interconnects.

#128648 - $15.00 USD Received 18 May 2010; revised 7 Aug 2010; accepted 19 Oct 2010; published 29 Oct 2010

High-power VCSEL array representing an attractive light source for various field of medium to high-power applications such as pumping the solid-state and fiber lasers is widely reported [4,5]. However, for optical pumping of solid-state and fiber lasers, there are stringent requirements on the high power and good-beam quality of the pump source. In this case, uniform 2-D microlens improving the beam quality with the same footprint as the VCSEL array is necessary. Up to now, various fabrication techniques for monolithic microlens-integrated VCSELs, such as photoresist reflow followed by dry-etching [6], focused ion beam milling [7], mass transport after pre-shaping [8], and shadow mask re-growth [9] have been reported. Yet, those methods require multiple process steps or expensive processing equipments. Meanwhile, individual microlens array is not easy to integrate with the mass VCSEL array exactly.

In this letter, a novel fabrication of microlens by using one-step diffusion-limited wet-etching techniques on the emitting VCSEL array windows is demonstrated. The integration of GaAs microlens directly on the substrate of VCSEL can still offer large alignment tolerance, accompanied with the advantages of simple and compact device packaging.

2. Structure of microlens-integrated VCSEL array

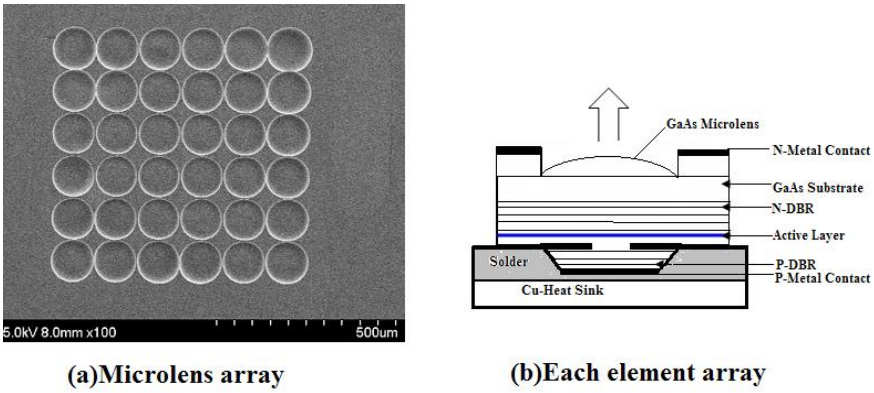

Fig. 1. (a) Microlens array by one-step diffusion-limited wet-etching techniques with the nominal diameter of each element about 100μm. (b) Schematic diagram of microlens-integrated 980nm bottom-emitting oxide-confined element array.

The schematic cross-section of microlens-integrated bottom-emitting 980nm VCSEL array is illustrated in Fig. 1. The overall size of the microlens-integrated 6 × 6 VCSEL array consisting of 36 elements with 120μm center-to-center-spacing is about 1mm × 1mm × 0.2mm. The diameter of the active layer of each element array is about 90μm, and the emitting window of that is 100μm. The epitaxy wafer is grown on (100) GaAs substrate by using low-pressure metal organic chemical vapor deposition (MOCVD) with the active region consisting of three $In_{0.2}Ga_{0.8}As$ (6nm)/$Ga_{0.18}As_{0.82}P$(8nm) quantum wells emitting the wavelength of 980nm, which are embedded in 10nm thick GaAs barriers and surrounded by AlGaAs claddings. The highly reflective p-type distributed Bragg Reflector (DBR) is built of 30 pairs of quarter-wavelength thick $Al_{0.9}Ga_{0.1}As$/GaAs with a graded interface providing 99.9% reflectivity. To reduce the series resistance of p-DBR, carbon as a p-type dopant is employed using extra modulated doping near interface to decrease the voltage drop without increasing absorption losses. There is a 30nm thick AlAs layer located above the p-type cladding layer for selective oxidation, which can supply lateral confinement to the current and light after AlAs is oxidized and converted into Al_xO_y layer. The n-type Si-dopped Bragg stack is composed of 22 pairs $Al_xGa_{1-x}As$ providing 99.2% reflectivity. The 30nm thick AlAs layer is oxidized about 10 minutes at 420°C under nitrogen gas bubbled through water at 95°C to form current apertures with oxidation depths from 8μm~10μm. The surface is passivated with Al_2O_3 and a circular window on the top of the mesa is opened for evaporating a full size P-

#128648 - $15.00 USD Received 18 May 2010; revised 7 Aug 2010; accepted 19 Oct 2010; published 29 Oct 2010

type contact consisting of Ti-Au-Pt-Au to provide a homogeneous current distribution and serve as a metal pad for soldering.

A 100-nm-thick SiO_2 masking layer has been deposited on GaAs substrate firstly, and then circular hole with an appropriate diameter is formed on the SiO_2 masking layer by standard photolithography in order to expose the emitting window. The patterned samples are immersed in a diffusion-limited etchant, which is composed of HBr, H_2O_2, and H_2O in the ratio of 1:1:15 at the static environment [10]. Due to the low mobility of Br_2 molecular, Br_2 molecular near the edge of circular hole is consumed much faster than in the center of circular hole. Such the spatial variation in the etching rate across the emitting window forms a spherical profile on the surface of substrate. The lens curvature radius is dependent on the etching time and the composition ratio of the solution. In addition, the etching progress should set in the static environment because any disturbance against the nature diffusive motion of the etching species would alter the details of microlens. The atomic force microscope (AFM) technique is employed to quantitatively evaluate the surface profile of microlens. The curvature radius of microlens of 959.9μm and the focal length of 369.2μm are achieved, and the root-mean-square roughness of the whole microlens surface is about 11.8nm. After fabricating microlens array by this method, emitting windows is opened by standard lift-off process, which is surrounded by the large-area Ge-Au-Ni-Au electrical contact. The annealing process is carried out at 420°C in a nitrogen environment for about 60 seconds. Finally, the device is precise soldered upon a copper heat sink with indium solder. The total thickness of the device is about 200μm with polished surface on the N^+-GaAs substrate to reduce the scattering loss.

3. Results and discussions

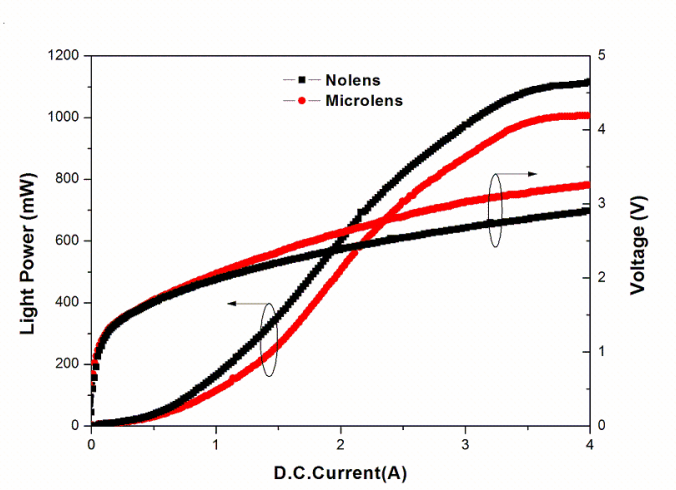

Fig. 2. L-I and V-I characteristics of microlens- integrated and conventional VCSEL array at a current of 4A D.C.

The threshold current, threshold voltage and differential resistance of microlens-integrated device, shown in the Fig. 2, are 0.96A, 2.04V and 0.41Ω, respectively. A maximum output power under CW operation is above 1W corresponding to a power density of 0.44kW/cm^2 at room temperature, which is limited by thermal roll. The maximum slop efficiency is 0.36W/A, which is greatly lower due to much more internal heating in the active region. Yet, the L-I, V-I characteristics of the ordinal VCSEL without microlens seems better than microlens-integrated device. A maximum output power, the threshold current, threshold voltage and differential resistance of ordinal device without microlens are 1.17W, 0.79A, 1.96V and 0.39Ω, respectively. The output power of conventional device is a little higher than that of microlens-integrated device because of deposition an antireflection coating (AR) on

#128648 - $15.00 USD Received 18 May 2010; revised 7 Aug 2010; accepted 19 Oct 2010; published 29 Oct 2010

the emitting windows, which can reduce some reflectivity for the conventional device in favor of improving the output power. Due to the microlens on GaAs substrate, the equivalent reflectivity R'_{bot} of n-DBR should be slightly increased, meanwhile, the effective cavity length is elongated, and the relatively larger roughness of the microlens surface creates additional scattering losses. It can be concluded that the threshold current of microlens-integrated VCSEL array (0.96A) could be a little higher than that of conventional VCSEL device (0.79A) without microlens according to the following empirical formula:

$$I_{th} = \frac{eMV_a}{\eta_i \tau_{sp}} N_{tr} \exp\{\frac{1}{ML_z}[L_{eff}\alpha_i + \frac{1}{2}\ln(\frac{1}{R_{top}R'_{bot}})]\},$$

where e, M, V_a, η_i, τ_{sp}, N_{tr}, Lz, L_{eff}, α_i, R_{top}, and R'_{bot} are the charge of electron, the number of quantum wells, the volume of the active region, the internal quantum efficiency, the carrier lifetime, the transparent carrier density, the width of quantum well, the effective cavity length, the total loss of scattering and absorption, the reflectivity of p-DBR, and the equivalent reflectivity of n-DBR and microlens.

#128648 - $15.00 USD Received 18 May 2010; revised 7 Aug 2010; accepted 19 Oct 2010; published 29 Oct 2010

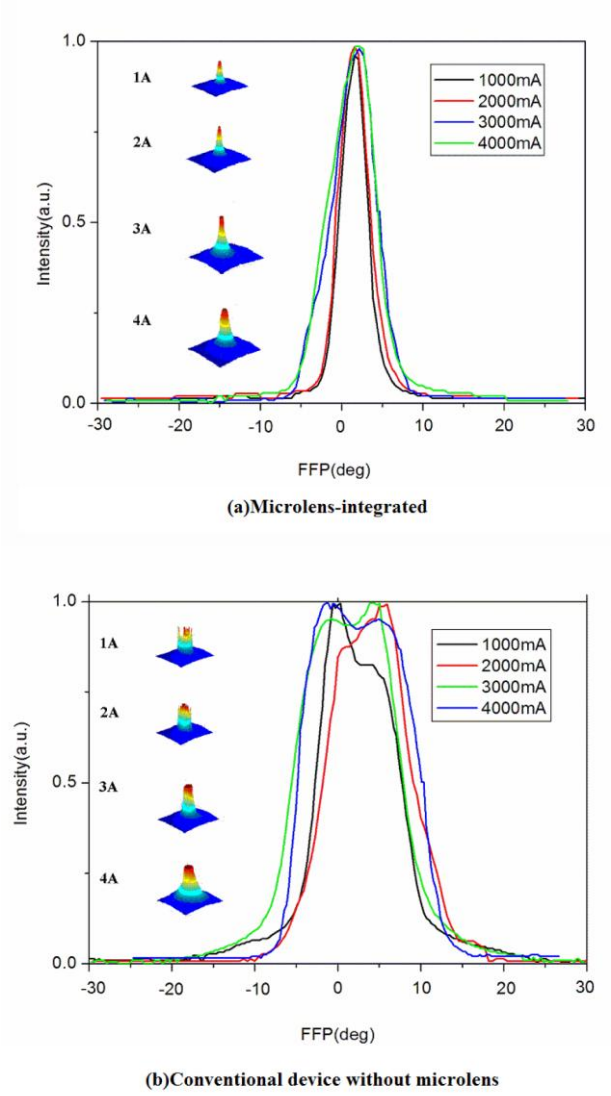

Fig. 3. Comparison of far-field distribution of microlens-integrated and conventional VCSEL array at different driving currents. The inset of each figure is the far-field lasing intensity distribution under different currents.

The obvious improvement is the far-field beam divergence of 6.6°[full-width at half-maximum(FWHM)] for microlens-integrated VCSEL array compared to the beam divergence of 14.8° for conventional VCSEL device without the microlens at a current of 4A, as shown in the green line of Fig. 3(a) and (b). It is in good agreement with theoretical value of 6° for microlens-integrated device according to our design before. The far-field characteristics of microlens-integrated device are much better than conventional device in the whole range of operating currents from 1A to 4A. The far-field divergences of microlens-integrated device are 3.7°, 4.5°, 5.9°, 6.6°, when operating currents are 1000mA, 2000mA, 3000mA, 4000mA, respectively. Yet, the far-field beam divergences of conventional device are 10.3°, 10.9°, 13.4°, and 14.8° at the different operating currents from 1000mA to 4000mA. The convex GaAs-microlens can introduce a small additional reflectivity when the light travels through the microlens, so the light emitted out of the n-DBR is partly reflected by the surface of the convex microlens back into the active region. The fed-back light overlaps in the quantum well

#128648 - $15.00 USD Received 18 May 2010; revised 7 Aug 2010; accepted 19 Oct 2010; published 29 Oct 2010

active layer. The total accumulative field strength that the quantum well active layer experiences is therefore spatially concentrated toward the aperture center, which can effectively reduce the far-field beam divergence [11]. Far-field lasing intensity distributions for both devices are illustrated in the inset of Fig. 3 (a) and (b) above threshold current. The beam quality of microlens-integrated device seems much better than that of conventional device in the whole range of operating currents from 1A to 4A. Although the beam quality will be deteriorated as increasing the operating current, which is caused by the current crowding due to the ring shape of n-contact, the microlens-integrated device could always keep excellent beam quality whenever the device operates in lower or higher currents. Owing to the circularly symmetric far-field distribution with lower beam divergence, the beam of microlens-integrated VCSEL array can be easily collimated into a fiber in a simple butt-coupling arrangement.

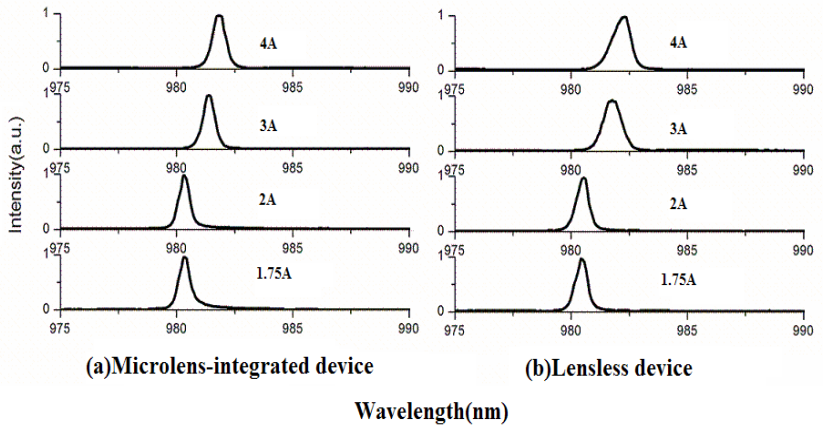

Fig. 4. Spectral performance between microlens-integrated VCSEL array and conventional VCSEL array at different operating currents.

Figure 4 shows that the peak wavelength of microlens-integrated VCSEL array is about 981.7nm with the FWHM of the spectrum is 0.7nm at a current of 4A, and that of conventional VCSEL array is 982.3nm with the FWHM of spectrum is 0.9nm at the same condition. As is expected, the spectrum shifts toward longer wavelengths with increasing drive current for microlens-integrated device (0.79nm/A) and conventional VCSEL device (0.88nm/A). The spectrum envelope width of conventional device (0.9nm) is a bit higher than that of microlens-integrated device (0.7nm). The main reason is that the fabrication of microlens on the substrate can bring additional weak optical feedback, which can suppress higher order transverse mode lasing effectively. As a result, the conventional device operates in higher order transverse modes compared to microlense-integrated device; high heat generation will be achieved in the active region under the same package. Thus, the red-shift of conventional device is larger than that of microlens-integrated device with the operating current increased.

4. Conclusion

Microlens-integrated bottom-emitting VCSEL array is achieved with diffusion-limited wet-etching technique. The maximum CW output power of 1W is obtained at room temperature. The peak wavelength is 981.7nm and the FWHM of the spectrum is 0.7nm. The microlens-integrated device improves greatly the far field distribution profile with much smaller beam divergence of 6.6°.

Acknowledgment

This work is supported by the National Natural Science Foundation of China (NNSFC) under Grant No. 60636020, 60676034, 60476029, 60577003, 60876036, and 60706007.

#128648 - $15.00 USD Received 18 May 2010; revised 7 Aug 2010; accepted 19 Oct 2010; published 29 Oct 2010